Editors' Suggestion | Featured in Physics

Cluster-Decorated Lieb Lattice: A Convenient and Reliable Platform for Tuning Flat-Band Energy

H. T. Li,[1,*] W. L. Fan,[1,*] Z. X. Zhang,[1] R. G. Yan,[1] T. Z. Ji,[1] S. Y. Wang,[1] L. Sun,[1] G. Chen,[1] B. F. Miao,[1] and H. F. Ding[1,2,3,†]

[1]National Laboratory of Solid State Microstructures, Department of Physics, and Collaborative Innovation Center of Advanced Microstructures, Nanjing University, Nanjing 210093, China
[2]Jiangsu Key Laboratory of Quantum Information Science and Technology, Nanjing University, Suzhou 215163, China
[3]Shishan Laboratory, Nanjing University, Suzhou 215163, China

(Received 18 December 2025; revised 4 June 2026; accepted 25 August 2026; published 20 October 2026)

Combining tight-binding theory, atom manipulation, and scanning tunneling spectroscopy, we demonstrate a quasicontinuous tuning of the flat-band energy in cluster-decorated Lieb lattices. By substituting the edge sites of Lieb lattices with tunable, rhombus-shaped four-site clusters, the emergent flat bands inherit the eigenenergies of the clusters and can be smoothly and predictably adjusted over a wide range, as verified experimentally with Fe atomic lattices on Ag(111). Our approach enables precise alignment of the flat-band energy with the Fermi level while preserving graph connectivity, providing a convenient and reliable platform for exploring emerging phenomena in quantum materials.

DOI: 10.1103/rm6q-k54p

Flat bands, characterized by their vanishingly small energy dispersion, have emerged as a central focus of contemporary research due to their remarkable capability to host exotic quantum states [1–18]. These fascinating properties arise from the divergent density of states and quenched kinetic energies. When situated near the Fermi level (E_F), flat bands can significantly enhance many-body interactions, thereby promoting novel correlated phases [19–24]. A notable example is flat-band-assisted superconductivity [21,25–27], where interband scattering between dispersive and flat bands plays a crucial role. This mechanism is notably exemplified in twisted bilayer graphene at specific "magic angles" [28,29], where a preferred band configuration, a flat band closely aligned with E_F, underpins the enhancement of the critical temperature. Numerous studies have successfully achieved tunable flat bands in twisted systems, demonstrating their strong potential [30–34].

In contrast, generating and controlling flat bands in other two-dimensional systems, particularly in artificial lattices constructed via atom manipulation, remains comparatively underdeveloped, despite the versatility and atomic-level precision that such platforms offer. Recent progress includes the direct construction of flat-band lattices [35,36], the symmetry-guided creation of flat bands [37], and a band-compression mechanism [38]. These developments lay a foundation for on and off control of flat bands. Exploring the rich landscape of flat-band-induced phenomena, however, requires continuous control over their energy positions, particularly the capability to align a flat band with the Fermi level. Among the numerous theoretical frameworks for flat-band construction [1,13,39–47], several explicitly support control of the flat-band energy, including strain [39], hopping engineering [40,42], magnetic flux [13], optimization method [43], supersymmetric transformation [44], and compact localized states method [41,45]. While each method introduces tunable parameters, identifying experimentally accessible regimes remains challenging.

Here, utilizing tight-binding calculations, we propose an effective method to achieve quasicontinuous control of flat-band energies by replacing the edge sites of a Lieb lattice with rhombus-shaped four-atom clusters. We further experimentally demonstrate its feasibility utilizing Fe adatoms on the Ag(111) surface. The approach splits the original one flat band of a Lieb lattice into five flat bands, two of which are degenerate. Interestingly, these four flat-band energies are aligned with the eigenenergies of the cluster. By manipulating the dimension of the rhombus, the eigenenergies of the cluster change. So do the flat-band energies of the cluster-decorated Lieb Lattice. In such a way, the flat-band energies can be readily tuned with the dimension of the cluster. With atom manipulation, we construct various cluster-decorated Lieb lattices with different configurations, showcasing the generation of the flat bands and quasicontinuous manipulation of their energies. Remarkably, this includes the ability to align one flat band to the Fermi level. Our method opens up new possibilities for achieving highly tunable flat bands, paving the way for further exploration of exotic quantum physics and strongly correlated phenomena.

*These authors contributed equally to this work.
†Contact author: hfding@nju.edu.cn

 © 2026 American Physical Society

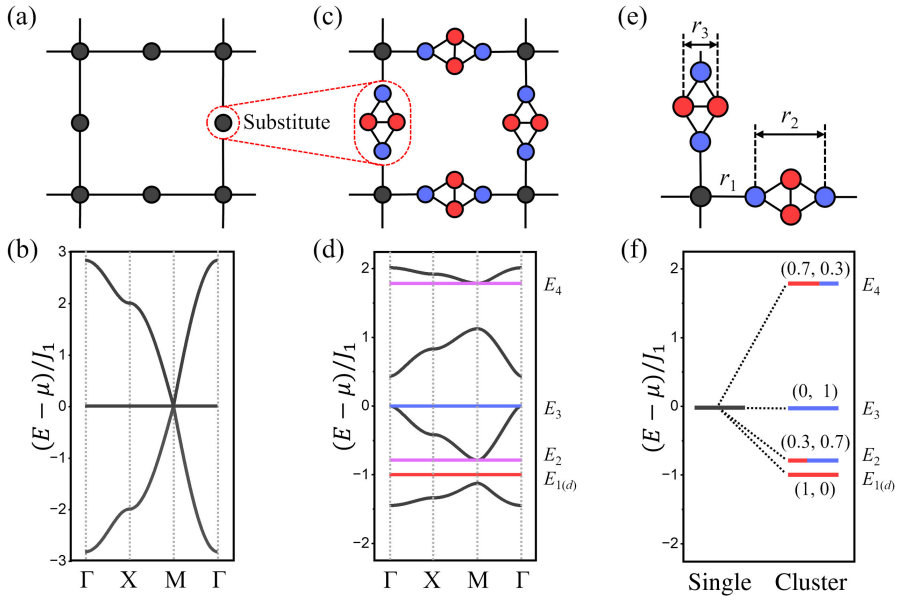


FIG. 1. (a) Schematic of a Lieb lattice. (b) Band structure of the Lieb lattice in (a), featuring a flat band at the on-site energy, μ. J_1 denotes the nearest-neighbor hopping. (c) Schematic of a cluster-decorated Lieb lattice, where the edge sites of the Lieb lattice are replaced by rhombus-shaped clusters. (d) Band structure of the cluster-decorated Lieb lattice, including four flat bands. In it, $r_1 : r_2 : r_3 = 2 : 3.6 : 1.5$ with r_1, r_2, and r_3 defined in (e). For simplicity, we limit our discussion for $r_3 < r_1, r_2$. (f) Origin of the flat bands shown in (d): replacement of the edge site by a four-site cluster yields five flat bands that inherit the eigenenergies of the cluster. They are marked by the distribution of the density of states on the corresponding types of sites. The difference of μ at different sites will shift the relative position of the flat bands. $\mu_{m/s} = \mu$ is assumed in the figure for brevity.

The Lieb lattice [Fig. 1(a)] represents a typical flab-band lattice [48]. The band structure features a flat band located at the on-site energy when only the nearest-neighbor interactions are considered [Fig. 1(b)] [49]. This flat band originates from the destructive interference, which gives rise to localized states residing on the edge sites [36]. Replacing the edge sites with rhombus-shaped four-atom clusters, as depicted in Fig. 1(c), a special lattice called a cluster-decorated Lieb lattice can be created. Several examples have also been theoretically identified in the flat-band lattice database [43]. In our construction, the four-site cluster comprises two distinct types of sites: the "side sites" (blue spheres), which connect to the corner sites of the lattice, and the "middle sites" (red spheres), located in the middle line between two neighboring corner sites.

The cluster-decorated Lieb lattice can be parametrized by three key parameters [Fig. 1(e)]: the separation between the side sites and the corner sites of the lattice, r_1, and the distance between two side sites or middle sites, r_2 and r_3. These lattices exhibit distinctive and robust features. Notably, the system supports five flat bands, $E_{1(d)}$ (two degenerate flat bands), E_2, E_3, and E_4, as shown in Fig. 1(d). The energies of these flat bands are precisely aligned with the eigenenergies of an isolated cluster with the same dimension. This can be viewed as a natural extension of the flat-band formation mechanism in the original Lieb lattice, where the destructive interference effectively decouples the edge sites from the rest of the system [40,46]. Replacing the edge sites with four-site clusters lifts the degeneracy and produces four distinct energy levels [Fig. 1(f)], which correspond to the flat-band energies in the cluster-decorated Lieb lattice. The one-to-one correspondence between cluster eigenenergies and flat-band energies provides a convenient and tunable platform for flat-band engineering, as the flat-band positions can be readily adjusted through geometric modification of the cluster.

The underlying physics can be understood as follows. Assuming zero hopping between the two side sites, the Hamiltonian of the rhombus-shaped four-site cluster can be written as

$$H_C = \begin{pmatrix} \mu_m & J_{m,m} & J_{m,s} & J_{m,s} \\ J_{m,m} & \mu_m & J_{m,s} & J_{m,s} \\ J_{m,s} & J_{m,s} & \mu_s & 0 \\ J_{m,s} & J_{m,s} & 0 & \mu_s \end{pmatrix}. \quad (1)$$

In it, $\mu_{m/s}$ is the on-site energy of middle sites or side sites, $J_{m,m}$ is the hopping constant between two middle sites, and $J_{m,s}$ is the hopping constant between a middle site and a side site. Solving the secular equation yields four discrete eigenenergies, as marked in Fig. 1(f),

$$\begin{cases} E_{1(d)} = \mu_m - J_{m,m} \\ E_2 = \frac{1}{2}\mu_m + \frac{1}{2}\mu_s + \frac{1}{2}J_{m,m} - \frac{1}{2}\sqrt{{J_{m,m}}^2 + 16{J_{m,s}}^2} \\ E_3 = \mu_s \\ E_4 = \frac{1}{2}\mu_m + \frac{1}{2}\mu_s + \frac{1}{2}J_{m,m} + \frac{1}{2}\sqrt{{J_{m,m}}^2 + 16{J_{m,s}}^2} \end{cases}. \quad (2)$$

As the hopping amplitude depends on the corresponding intersite distance, these four energies are functions of $\mu_{m/s}$, r_2, and r_3. Writing down the Hamiltonian of the cluster-decorated Lieb lattice, we find that these energies are also solutions of its secular equation [Supplemental Material (SM) Note 1 [50]]. This unique property provides an interesting route to control the flat-band energies by simply adjusting the cluster geometry and the on-site energy $\mu_{m/s}$. For convenience, we refer to these flat bands with their corresponding energies.

To verify this proposal, we performed experiments using a low-temperature scanning tunneling microscopy system (see details in SM Note 2 [50]). We employed atom manipulation to construct cluster-decorated Lieb lattices, each consisting of 57 Fe adatoms on an Ag(111) substrate. Two representative examples are displayed in the top panels of Fig. 2. For the specific configuration shown in Fig. 2(a), $r_1 \approx 2.02$ nm, $r_2 \approx 3.72$ nm, and $r_3 \approx 1.64$ nm. Differential conductance (dI/dV) spectra were measured at selected adatom positions. To minimize the effects of minor lattice distortions, spectra from symmetry-equivalent sites were averaged. To reduce the influence of the tip effect, the measured dI/dV spectra were normalized by a reference spectrum taken atop an isolated single adatom on a wide terrace. The raw data and the normalization procedures are presented in SM Note 3 [50]. As shown in Fig. 2(b), the normalized dI/dV spectrum at the middle sites (red curve, top panel) exhibits a pronounced peak at ~55 mV, in good agreement with the calculated local density of states (LDOS) (bottom panel). Note that an additional Gaussian broadening of 17.35 meV is included in the calculations to reproduce the experimental broadening (see details in SM Note 4 [50]). The normalized spectrum at the side sites (blue curve, top panel) shows several weak peaks, in contrast to the pronounced one at the middle site. These weak peaks align with the corresponding LDOS shown below. The intensity comparison of these peaks is discussed in SM Note 1 [50]. Given the one-to-one correspondence of the experimental spectra with the calculated LDOS, we attribute the pronounced peak at the middle sites to the $E_{1(d)}$ flat band. In the spectrum obtained at the side sites, the two peaks, at ~84 meV and ~168 meV, correspond to the E_2 and E_3 flat bands. Considering its prominence, we focus on the $E_{1(d)}$ flat band in our discussions below.

Figures 2(c) and 2(d) present the results for another representative. In this configuration, $r_1 = 3.00$ nm, $r_2 = 4.50$ nm, and $r_3 = 2.00$ nm. The normalized dI/dV spectra at both middle- and side-sites show close similarity in the peak positions with the calculated LDOS for the corresponding sites, further supporting the above interpretation. Remarkably, both experiment and theory confirm the presence of a flat band almost at the Fermi level. Thus, our experiments provide direct and robust confirmation of the proposed cluster-based mechanism. The clear difference in $E_{1(d)}$ between the two geometries also showcases the tunability of the flat-band energies as proposed.

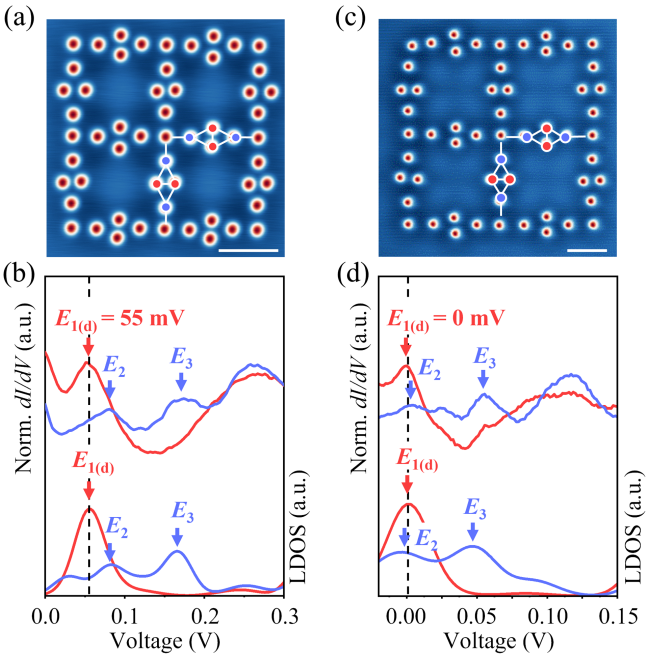


FIG. 2. Cluster-decorated Lieb lattices constructed with 57 Fe adatoms on Ag(111) surface and their electronic properties. (a) Topographic image of a cluster-decorated Lieb lattice with $r_1 \approx 2.02$ nm, $r_2 \approx 3.72$ nm, and $r_3 \approx 1.64$ nm. [(b), top] Normalized dI/dV spectra measured on the adatoms marked with corresponding colors in (a). [(b), bottom] Corresponding LDOS calculated using a tight-binding model with the same geometry. Note that both red curves obtained on the middle sites show a flat-band peak at ~55 mV. (c) and (d) are similar to (a) and (b) but with a different set of lattice parameters, $r_1 = 3.00$ nm, $r_2 = 4.50$ nm, and $r_3 = 2.00$ nm. Notably, both red curves show a flat-band peak at E_F. The scale bars in (a) and (c) are both 5 nm.

To further demonstrate the tunability of flat bands in cluster-decorated Lieb lattices, we assembled a series of such lattices with varying parameters and systematically investigate the dependence of $E_{1(d)}$ on r_1, r_2, and r_3. Following the same procedure described above, we extract the peak positions corresponding to the $E_{1(d)}$ flat band for each lattice. For the r_1 dependence, we varied r_1 from 1.50 to 3.50 nm while fixing $r_2 = 3.60$ nm and $r_3 = 1.50$ nm. The $E_{1(d)}$ flat band peak rapidly decreased from ~106 to −4 mV with increasing r_1 [Fig. 3(a)]. For the r_2 dependence, we fixed $r_1 = 2.00$ nm and $r_3 = 1.50$ nm; in this

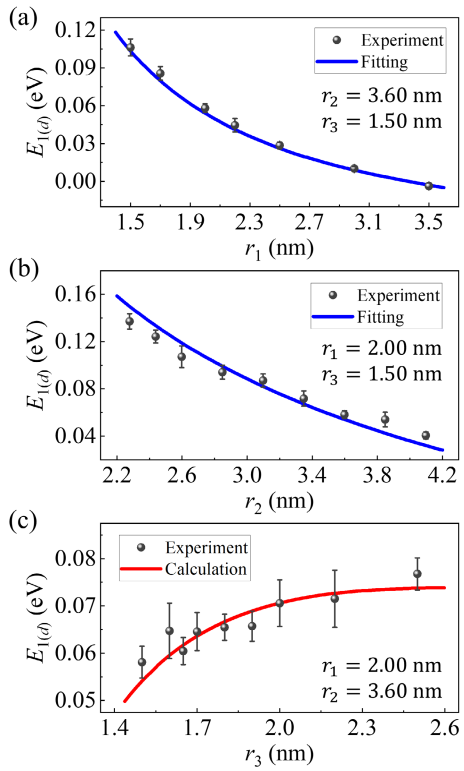


FIG. 3. Tuning the energy of the $E_{1(d)}$ band by modifying r_1, r_2, and r_3. Dark gray spheres represent the experimental data. Error bars indicate the standard deviation of the statistics. In (a) and (b), the blue solid lines are fits using Eq. (3), while the red curve in (c) is calculated using Eq. (3) with parameters obtained from fits in (a) and (b).

case, $E_{1(d)}$ also rapidly decreased from ~135 to ~40 mV with increasing r_2 [Fig. 3(b)]. The r_3 dependence of $E_{1(d)}$ in Fig. 3(c), which was obtained by maintaining $r_1 = 2.00$ nm and $r_2 = 3.60$ nm, however exhibited the opposite behavior. It increased with increasing r_3, and the amplitude of the variation is smaller, from ~55 to ~75 meV only.

In the following, we discuss the origin of these three dependencies. In our tight-binding calculations, $E_{1(d)}$ is primarily determined by μ_m and the overlap integral $J_{m,m}$. Previous investigations show that μ scales with the local atomic density and the hopping energy between two Fe adatoms on Ag(111) is a function of their separation r, which follows $J(r) = C_\Delta/r^2$ with $C_\Delta = 0.24$ eV/nm^2 [12]. To address the spatial inhomogeneity of atomic density, two additional assumptions are introduced: (1) effective-area assumption and (2) cluster assumption. For effective-area assumption, since each unit cell has the area of $(2r_1 + r_2)^2$ and the atoms are distributed away from the cell center, the effective area is defined as $S_{\text{eff}} = (2r_1 + r_2)^2 - r_2^2$. For cluster assumption, the on-site energy is further influenced by the presence of clusters due to their distinct local atomic configuration. Each rhombus-shaped cluster occupies an area of $\frac{1}{2}r_2r_3$ and a unit cell contains nine sites, eight of which form two rhombuses. Combining these effects with the influence of the surface state, we express the on-site energy as $\mu_p = \mu_0 + [9C_g/(2r_1 + r_2)^2 - r_2^2] + (8C_{1,p}/r_2r_3) + C_{2,p}\sum_{\Delta r}(1/\Delta r^2)$, where p denotes *middle* (m), *side* (s), or *corner* (c) sites. Here, μ_0 represents the on-site energy of the Ag(111) surface state. The C_g term describes the global contribution associated with the effective atomic density within the unit cell and is fixed at 0.633 eV nm^2 based on previous studies [38]. The parameters $C_{1,p}$ and $C_{2,p}$ describe the contributions from the local atomic configuration to the on-site energy. Δr denotes the distances between any other atoms and the investigated adatom, and a cutoff of 20 nm is applied, beyond which the contribution becomes negligible. Taking this on-site energy, we can further obtain the energy for $E_{1(d)}$ flat band as

$$E_{1(d)} = \mu_0 + \frac{9C_g}{(2r_1 + r_2)^2 - r_2^2} + \frac{8C_{1,m}}{r_2r_3} + C_{2,m}\sum_{\Delta r}\frac{1}{\Delta r^2} - \frac{C_\Delta}{r_3^2}. \tag{3}$$

We use Eq. (3) to fit the experimentally obtained r_1 and r_2 dependencies in Fig. 3. Interestingly, both datasets are well described using almost identical fitting parameters $C_{1,m}$ and $C_{2,m}$. The fitting yields $C_{1,m} = 0.089 \pm 0.005$ eV nm^2, $C_{2,m} = -0.012 \pm 0.003$ eV nm^2. Using the obtained $C_{1,m}$ and $C_{2,m}$, we further calculated the r_3 dependence. As shown in Fig. 3(c), the calculated curve (red line) quantitatively reproduces the experimental data (dark gray spheres), supporting the validity of the proposed model. We also fit $C_{1,s}$ and $C_{2,s}$ using the same model, and find that the E_3 flat-band peak can be also well reproduced (see SM Note 5 [50]).

Positioning the flat band near E_F is essential for the emergence of strong correlation effects and thus highly desired. This can be achieved through solving Eq. (3) for $E_{1(d)} = 0$. We find that $E_{1(d)}$ shows a weak dependence on r_2 when $r_1 = 3.00$ nm and $r_3 = 2.00$ nm, allowing a fine-tuning. And r_2 is calculated to be 4.54 nm for $E_{1(d)} = 0$. Varying r_2 around this value indeed tunes the flat band across the Fermi level, Fig. 4(a). This demonstrates that our approach can tune the flat-band energy and align it with the Fermi energy. Interestingly, as shown in SM Note 4 [50], we find that when the flat-band energy lies within ~20 meV of E_F, the width of the flat-band peak decreases rapidly and pronouncedly, in line with previous investigations [51,56]. This observation suggests a possible strong correlation effect though other mechanisms may also be involved. Further investigation, such as the temperature- and field-dependent phase transition studies, may be helpful to further clarify its origin.

Above, we demonstrated how each structural parameter can be utilized to control the flat bands in cluster-decorated Lieb lattices. If the lattice parameters are not adjusted appropriately, the lattice may fragment into several isolated

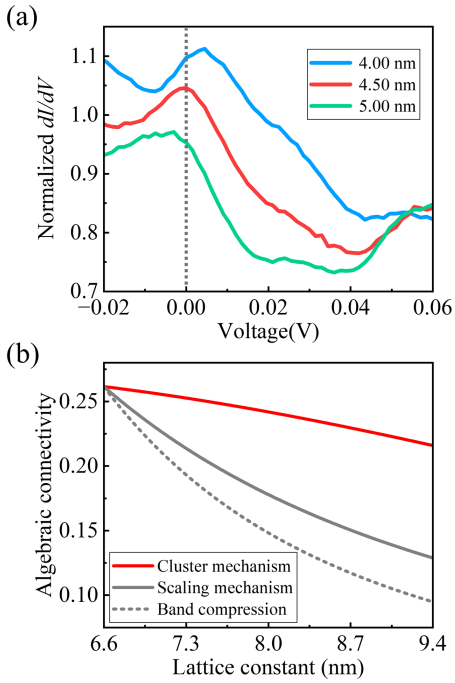


FIG. 4. (a) Tuning the flat-band energy near the Fermi level by varying r_2 in cluster-decorated Lieb lattices with $r_1 = 3.00$ nm and $r_3 = 2.00$ nm. The dashed line indicates the Fermi level. (b) Algebraic connectivity of the lattices as a function of lattice constant for different tuning mechanisms: the cluster mechanism (this Letter), the scaling mechanism (uniform lattice rescaling), and the band-compression approach [38].

parts, causing the flat bands to collapse into discrete energy levels [57–60]. Based on this insight, we compare three distinct mechanisms for tuning flat bands: (1) the cluster mechanism, where varying r_2 modifies the flat-band energies in cluster-decorated Lieb lattices; (2) the scaling mechanism, where uniform rescaling of the entire lattice results in proportional shifts of all energy levels; and (3) the band-compression method, where varying the second nearest-neighbor distance modifies the flat bands. To quantitatively compare these mechanisms, we employ graph-connectivity analysis (see details in SM Note 6 [50]), which is as a powerful tool in the study of flat-band systems [1,61–69]. The algebraic connectivity is defined as the second-smallest eigenvalue of the Laplacian matrix associated with the lattice graph [66,70,71]. A nonzero value indicates that the lattice remains connected, whereas a value of zero corresponds to a completely disconnected structure. Larger values imply stronger global interactions. Figure 4(b) depicts the algebraic connectivity as a function of the lattice constant for these three mechanisms. Though the connectivity decreases with increasing lattice constant in these three cases, the reduction for the cluster mechanism is significantly weaker, displaying only a relatively modest decrease. Importantly, it shows a nonzero value over a wide range. This demonstrates the preservation of algebraic connectivity. We note that a nonzero algebraic connectivity demonstrates graph connectivity but is not direct evidence of stronger many-body interactions or guaranteed preservation of the flat band.

In summary, we have demonstrated a convenient and reliable platform for the quasicontinuous and predictable tuning of flat-band energies using cluster-decorated Lieb lattices. By harnessing the intrinsic eigenenergies of tunable atomic clusters, this approach enables the formation of flat bands with predefined energy positions. We experimentally verified this approach through scanning tunneling spectroscopy on Fe-based atomic lattices on Ag(111), in particular, the ability to align a flat band precisely with the Fermi level. Moreover, graph-connectivity analysis reveals that the lattice retains strong structural coherence during tuning. Interestingly, we find our strategy can be generalized to other clusters as well as different mother flat-band lattices (SM Note 7 [50]). These results not only establish a robust experimental platform for flat-band engineering but also pave the way for future studies of exotic correlated phenomena.

Acknowledgments—This work is supported by the National Key R&D Program of China (Grants No. 2024YFA1408500, No. 2022YFA1403601, and No. 2023YFC2410501), the National Natural Science Foundation of China (Grants No. 12474059, No. 12241402, No. 12522404, No. 12274203, No. 12374113, and No. 12274204). Quantum Science and Technology-National Science and Technology Major Project No. 2024ZD0301102. The calculations are made in e-Science Center of Collaborative Innovation Center of Advanced Microstructures. H. T. L. acknowledges the support by the Nanjing University PhD Student Zhujian Program. G. C. acknowledges support by the Program for Innovative Talents and Entrepreneur in Jiangsu (No. JSSCTD202408).

Data availability—The data that support the findings of this article are not publicly available. The data are available from the authors upon reasonable request.

[1] N. Regnault, Y. Xu, M.-R. Li, D.-S. Ma, M. Jovanovic, A. Yazdani, S. S. P. Parkin, C. Felser, L. M. Schoop, N. P. Ong, R. J. Cava, L. Elcoro, Z.-D. Song, and B. A. Bernevig, Catalogue of flat-band stoichiometric materials, Nature (London) **603**, 824 (2022).

[2] D. Leykam, A. Andreanov, and S. Flach, Artificial flat band systems: From lattice models to experiments, Adv. Phys. X **3**, 1473052 (2018).

[3] P. M. Neves, J. P. Wakefield, S. Fang, H. Nguyen, L. Ye, and J. G. Checkelsky, Crystal net catalog of model flat band materials, npj Comput. Mater. **10**, 39 (2024).

[4] H. Park *et al.*, Ferromagnetism and topology of the higher flat band in a fractional Chern insulator, Nat. Phys. **21**, 549 (2025).

[5] W. Yang, D. Zhai, T. Tan, F.-R. Fan, Z. Lin, and W. Yao, Fractional quantum anomalous Hall effect in a singular flat band, Phys. Rev. Lett. **134**, 196501 (2025).
[6] H. Lu, B.-B. Chen, H.-Q. Wu, K. Sun, and Z. Y. Meng, Thermodynamic response and neutral excitations in integer and fractional quantum anomalous Hall states emerging from correlated flat bands, Phys. Rev. Lett. **132**, 236502 (2024).
[7] L. Ye, S. Fang, M. Kang, J. Kaufmann, Y. Lee, C. John, P. M. Neves, S. Y. F. Zhao, J. Denlinger, C. Jozwiak, A. Bostwick, E. Rotenberg, E. Kaxiras, D. C. Bell, O. Janson, R. Comin, and J. G. Checkelsky, Hopping frustration-induced flat band and strange metallicity in a kagome metal, Nat. Phys. **20**, 610 (2024).
[8] J. G. Checkelsky, B. A. Bernevig, P. Coleman, Q. Si, and S. Paschen, Flat bands, strange metals and the Kondo effect, Nat. Rev. Mater. **9**, 509 (2024).
[9] L. Classen and J. J. Betouras, High-order van Hove singularities and their connection to flat bands, Annu. Rev. Condens. Matter Phys. **16**, 229 (2025).
[10] Y. E. Vekovshinin, L. V. Bondarenko, A. Y. Tupchaya, T. V. Utas, E. Wang, A. N. Mihalyuk, D. V. Gruznev, A. V. Zotov, and A. A. Saranin, High-order van Hove singularities in atomically thin kagome metal $LaTl_3$, ACS Nano **19**, 36510 (2025).
[11] X. Chen, L. Wang, J. Ishizuka, R. Zhang, K. Nogaki, Y. Cheng, F. Yang, Z. Chen, F. Zhu, Z. Liu, J. Mei, Y. Yanase, B. Lv, and Y. Huang, Coexistence of near-E_F flat band and van Hove singularity in a two-phase superconductor, Phys. Rev. X **14**, 021048 (2024).
[12] R.-G. Yan, Z.-X. Zhang, T.-Z. Ji, W.-L. Fan, H.-T. Li, L. Sun, B.-F. Miao, G. Chen, R. Wang, B.-G. Wang, and H.-F. Ding, Arbitrary positioning higher-order topological boundary states in Fe breathing-kagome lattices on Ag(111), Chin. Phys. Lett. **42**, 080710 (2025).
[13] B. Pal and G. Bouzerar, Engineering flux-controlled flat bands and topological states in a Stagome lattice, J. Phys. Condens. Matter **37**, 135503 (2025).
[14] X. Li, D. Wang, H. Hu, and Y. Pan, Designer artificial chiral kagome lattice with tunable flat bands and topological boundary states, Nanotechnology **35**, 145601 (2024).
[15] F. Liu, Y. Yan, W. Tang, B. Qie, J. Chen, Z. Wang, S. G. Louie, and F. R. Fischer, Orbital engineering band degeneracy in a dual-square carbon-oxide framework, ACS Nano **19**, 15139 (2025).
[16] M. R. Slot, S. N. Kempkes, E. J. Knol, W. M. J. van Weerdenburg, J. J. van den Broeke, D. Wegner, D. Vanmaekelbergh, A. A. Khajetoorians, C. Morais Smith, and I. Swart, *p*-band engineering in artificial electronic lattices, Phys. Rev. X **9**, 011009 (2019).
[17] S. N. Kempkes, M. R. Slot, J. J. van den Broeke, P. Capiod, W. A. Benalcazar, D. Vanmaekelbergh, D. Bercioux, I. Swart, and C. Morais Smith, Robust zero-energy modes in an electronic higher-order topological insulator, Nat. Mater. **18**, 1292 (2019).
[18] R. Yin, X. Zhu, Q. Fu, T. Hu, L. Wan, Y. Wu, Y. Liang, Z. Wang, Z.-L. Qiu, Y.-Z. Tan, C. Ma, S. Tan, W. Hu, B. Li, Z. F. Wang, J. Yang, and B. Wang, Artificial kagome lattices of Shockley surface states patterned by halogen hydrogen-bonded organic frameworks, Nat. Commun. **15**, 2969 (2024).
[19] K.-E. Huhtinen, J. Herzog-Arbeitman, A. Chew, B. A. Bernevig, and P. Törmä, Revisiting flat band superconductivity: Dependence on minimal quantum metric and band touchings, Phys. Rev. B **106**, 014518 (2022).
[20] J. Huang, L. Chen, Y. Huang, C. Setty, B. Gao, Y. Shi, Z. Liu, Y. Zhang, T. Yilmaz, E. Vescovo, M. Hashimoto, D. Lu, B. I. Yakobson, P. Dai, J.-H. Chu, Q. Si, and M. Yi, Non-Fermi liquid behaviour in a correlated flat-band pyrochlore lattice, Nat. Phys. **20**, 603 (2024).
[21] N. B. Kopnin, T. T. Heikkilä, and G. E. Volovik, High-temperature surface superconductivity in topological flat-band systems, Phys. Rev. B **83**, 220503(R) (2011).
[22] J.-X. Yin *et al.*, Negative flat band magnetism in a spin–orbit-coupled correlated kagome magnet, Nat. Phys. **15**, 443 (2019).
[23] S. Gao *et al.*, Discovery of a single-band Mott insulator in a van der Waals flat-band compound, Phys. Rev. X **13**, 041049 (2023).
[24] J. Hu, X. Zhang, C. Hu, J. Sun, X. Wang, H.-Q. Lin, and G. Li, Correlated flat bands and quantum spin liquid state in a cluster Mott insulator, Commun. Phys. **6**, 172 (2023).
[25] G. E. Volovik, Graphite, graphene, and the flat band superconductivity, JETP Lett. **107**, 516 (2018).
[26] A. Bussmann-Holder, H. Keller, A. Simon, and A. Bianconi, Multi-Band superconductivity and the steep band/flat band scenario, Condens. Matter **4**, 91 (2019).
[27] R. Khasanov, B.-B. Ruan, Y.-Q. Shi, G.-F. Chen, H. Luetkens, Z.-A. Ren, and Z. Guguchia, Tuning of the flat band and its impact on superconductivity in $Mo_5Si_{3-x}P_x$, Nat. Commun. **15**, 2197 (2024).
[28] S. Lisi *et al.*, Observation of flat bands in twisted bilayer graphene, Nat. Phys. **17**, 189 (2021).
[29] Y. Cao, V. Fatemi, S. Fang, K. Watanabe, T. Taniguchi, E. Kaxiras, and P. Jarillo-Herrero, Unconventional superconductivity in magic-angle graphene superlattices, Nature (London) **556**, 43 (2018).
[30] X. Liu, C.-L. Chiu, J. Y. Lee, G. Farahi, K. Watanabe, T. Taniguchi, A. Vishwanath, and A. Yazdani, Spectroscopy of a tunable moiré system with a correlated and topological flat band, Nat. Commun. **12**, 2732 (2021).
[31] L.-Z. Yang, L.-H. Tong, C.-S. Liao, Q. Wu, X. Fu, Y.-Y. Zhou, Y. Tian, L. Zhang, L. Zhang, M.-Q. Cai, L. He, Z. Qin, and L.-J. Yin, Origami-controlled strain engineering of tunable flat bands and correlated states in folded graphene, Phys. Rev. Mater. **6**, L041001 (2022).
[32] Y. Wang, J. Zhu, G. W. Burg, A. Swain, K. Watanabe, T. Taniguchi, Y. Zheng, A. H. MacDonald, and E. Tutuc, Independently tunable flat bands and correlations in a graphene double moiré system, Phys. Rev. Lett. **134**, 096204 (2025).
[33] B. L. Chittari, G. Chen, Y. Zhang, F. Wang, and J. Jung, Gate-tunable topological flat bands in trilayer graphene boron-nitride moire superlattices, Phys. Rev. Lett. **122**, 016401 (2019).
[34] L. Du, Z. Liu, S. J. Wind, V. Pellegrini, K. W. West, S. Fallahi, L. N. Pfeiffer, M. J. Manfra, and A. Pinczuk, Observation of flat bands in gated semiconductor artificial graphene, Phys. Rev. Lett. **126**, 106402 (2021).

[35] M. R. Slot, T. S. Gardenier, P. H. Jacobse, G. C. P. van Miert, S. N. Kempkes, S. J. M. Zevenhuizen, C. M. Smith, D. Vanmaekelbergh, and I. Swart, Experimental realization and characterization of an electronic Lieb lattice, Nat. Phys. **13**, 672 (2017).
[36] X. Li, Q. Li, T. Ji, R. Yan, W. Fan, B. Miao, L. Sun, G. Chen, W. Zhang, and H. Ding, Lieb lattices formed by real atoms on Ag(111) and their lattice constant-dependent electronic properties, Chin. Phys. Lett. **39**, 057301 (2022).
[37] M. N. Huda, S. Kezilebieke, and P. Liljeroth, Designer flat bands in quasi-one-dimensional atomic lattices, Phys. Rev. Res. **2**, 043426 (2020).
[38] R. G. Yan, T. Z. Ji, W. L. Fan, Z. X. Zhang, H. T. Li, L. Sun, B. F. Miao, G. Chen, and H. F. Ding, Experimental demonstration of the band compression effect in engineered kagome-honeycomb lattices, Phys. Rev. B **108**, 075153 (2023).
[39] Z. Bi, Noah F. Q. Yuan, and L. Fu, Designing flat bands by strain, Phys. Rev. B **100**, 035448 (2019).
[40] S. Flach, D. Leykam, J. D. Bodyfelt, P. Matthies, and A. S. Desyatnikov, Detangling flat bands into Fano lattices, Europhys. Lett. **105**, 30001 (2014).
[41] W. Maimaiti, A. Andreanov, and S. Flach, Flat-band generator in two dimensions, Phys. Rev. B **103**, 165116 (2021).
[42] T. Mizoguchi and M. Udagawa, Flat-band engineering in tight-binding models: Beyond the nearest-neighbor hopping, Phys. Rev. B **99**, 235118 (2019).
[43] H. T. Li, T. Z. Ji, R. G. Yan, W. L. Fan, Z. X. Zhang, L. Sun, B. F. Miao, G. Chen, X. G. Wan, and H. F. Ding, General method to construct flat bands in two-dimensional lattices, Phys. Rev. Lett. **134**, 076402 (2025).
[44] V. Jakubský and K. Zelaya, Flat-band engineering of quasi-one-dimensional systems via supersymmetric transformations, Phys. Rev. B **109**, 245406 (2024).
[45] A. Graf and F. Piéchon, Designing flat-band tight-binding models with tunable multifold band touching points, Phys. Rev. B **104**, 195128 (2021).
[46] R. G. Dias and J. D. Gouveia, Origami rules for the construction of localized eigenstates of the Hubbard model in decorated lattices, Sci. Rep. **5**, 16852 (2015).
[47] K. S. Thakur, V. Theuno, A. Mukherjee, and B. Pal, Proximity-induced flat bands and topological properties in a decorated diamond chain, J. Phys. Condens. Matter **37**, 475503 (2025).
[48] E. H. Lieb, Two theorems on the Hubbard model, Phys. Rev. Lett. **62**, 1201 (1989).
[49] R. Shen, L. B. Shao, B. Wang, and D. Y. Xing, Single Dirac cone with a flat band touching on line-centered-square optical lattices, Phys. Rev. B **81**, 041410(R) (2010).
[50] See Supplemental Material at http://link.aps.org/supplemental/10.1103/rm6q-k54p for details of the tight-binding model of cluster-decorated Lieb lattices, details of the experiment, experimental data, and processing, which includes Refs. [12,36,38–45,51–55].
[51] W. Li, Z. Yang, Z. Liu, Y. Xie, R. Zhong, F. Zheng, Y. Wu, J. Li, H. Xing, C. Wen, C. Si, and S. Yan, Emergence of the flat band and Kondo resonance in the superconducting T/H-NbS_2 heterostructure, ACS Nano **19**, 21962 (2025).
[52] Q. Li, X. Li, B. Miao, L. Sun, G. Chen, P. Han, and H. Ding, Kondo-free mirages in elliptical quantum corrals, Nat. Commun. **11**, 1400 (2020).
[53] D. Bonnell, *Scanning Probe Microscopy and Spectroscopy: Theory, Techniques, and Applications* (John Wiley & Sons, New York, 2000).
[54] S. Crampin and O. R. Bryant, Fully three-dimensional scattering calculations of standing electron waves in quantum nanostructures: The importance of quasiparticle interactions, Phys. Rev. B **54**, R17367 (1996).
[55] J. Jiang, Q. Gao, Z. Zhou, C. Shen, M. Di Luca, E. Hajigeorgiou, K. Watanabe, T. Taniguchi, and M. Banerjee, Direct probing of energy gaps and bandwidth in gate-tunable flat band graphene systems, Nat. Commun. **16**, 1308 (2025).
[56] E. Li, J.-X. Hu, X. Feng, Z. Zhou, L. An, K. T. Law, N. Wang, and N. Lin, Lattice reconstruction induced multiple ultra-flat bands in twisted bilayer WSe2, Nat. Commun. **12**, 5601 (2021).
[57] L. Balents, C. R. Dean, D. K. Efetov, and A. F. Young, Superconductivity and strong correlations in moiré flat bands, Nat. Phys. **16**, 725 (2020).
[58] V. R. Shaginyan, M. Y. Amusia, A. Z. Msezane, V. A. Stephanovich, G. S. Japaridze, and E. V. Kirichenko, Flat bands and salient experimental features supportingthe fermion condensation theory of strongly correlated Fermi systems, Phys. At. Nucl. **83**, 132 (2020).
[59] V. Peri, Z.-D. Song, B. A. Bernevig, and S. D. Huber, Fragile topology and flat-band superconductivity in the strong-coupling regime, Phys. Rev. Lett. **126**, 027002 (2021).
[60] G. Möller and N. R. Cooper, Correlated phases of bosons in the flat lowest band of the dice lattice, Phys. Rev. Lett. **108**, 045306 (2012).
[61] D.-S. Ma, Y. Xu, C. S. Chiu, N. Regnault, A. A. Houck, Z. Song, and B. A. Bernevig, Spin-orbit-induced topological flat bands in line and split graphs of bipartite lattices, Phys. Rev. Lett. **125**, 266403 (2020).
[62] H. Liu, G. Sethi, S. Meng, and F. Liu, Orbital design of flat bands in non-line-graph lattices via line-graph wave functions, Phys. Rev. B **105**, 085128 (2022).
[63] A. J. Kollár, M. Fitzpatrick, P. Sarnak, and A. A. Houck, Line-graph lattices: Euclidean and non-euclidean flat bands, and implementations in circuit quantum electrodynamics, Commun. Math. Phys. **376**, 1909 (2020).
[64] T. Ogata, M. Kawamura, and T. Ozaki, Methods for constructing parameter-dependent flat-band lattices, Phys. Rev. B **103**, 205119 (2021).
[65] E. Agliari, O. MÜLken, and A. Blumen, Continuous-time quantum walks and trapping, Int. J. Bifurcation Chaos **20**, 271 (2010).
[66] I. Gutman, in *Advances in Quantum Chemistry*, edited by J. R. Sabin and E. Brändas (Academic Press, New York, 2006), pp. 125.
[67] E. V. Miu, J. R. McKone, and G. Mpourmpakis, Global and local connectivities describe hydrogen intercalation in metal oxides, Phys. Rev. Lett. **131**, 108001 (2023).

[68] L. Dal Negro, D. T. Henderson, and F. Sgrignuoli, Wave transport and localization in prime number landscapes, Front. Phys. **9**, 723456 (2021).

[69] A. Jahanbani, S. M. Sheikholeslami, and S. Filipovski, Relations between the energy and topological indices of a graph, Mediterr. J. Math **20**, 264 (2023).

[70] M. Fiedler, Algebraic connectivity of graphs, Czech. Math. J. **23**, 298 (1973).

[71] N. M. M. de Abreu, Old and new results on algebraic connectivity of graphs, Linear Algebra Appl. **423**, 53 (2007).